

Simulation of Quantum Adiabatic Search in the Presence of Noise

Frank Gaitan

Department of Physics; Southern Illinois University; Carbondale, IL 62901-4401

(Dated: August 8, 2018)

Results are presented of a large-scale simulation of the quantum adiabatic search (QuAdS) algorithm in the presence of noise. The algorithm is applied to the NP -Complete problem N -Bit Exact Cover 3 (EC3). The noise is assumed to Zeeman-couple to the qubits and its effects on the algorithm's performance is studied for various levels of noise power, and for 4 different types of noise polarization. We examine the scaling relation between the number of bits N (EC3 problem-size) and the algorithm's noise-averaged median run-time $\langle T(N) \rangle$. Clear evidence is found of the algorithm's sensitivity to noise. Two fits to the simulation results were done: (1) power-law scaling $\langle T(N) \rangle = aN^b$; and (2) exponential scaling $\langle T(N) \rangle = a[\exp(bN) - 1]$. Both types of scaling relations provided excellent fits, although the scaling parameters a and b varied with noise power, and with the type of noise polarization. The sensitivity of the scaling exponent b to noise polarization allows a relative assessment of which noise polarizations are most problematic for quantum adiabatic search. We demonstrate how the noise leads to decoherence in QuAdS, and estimate the amount of decoherence present in our simulations. An upper bound is also derived for the noise-averaged QuAdS success probability in the limit of weak noise that is appropriate for our simulations.

PACS numbers: 03.67.Lx, 03.65.Yz, 05.40.Ca

I. INTRODUCTION

In computational complexity theory [1], computational problems are classified according to the resources needed to obtain a solution. Often such a problem is reformulated as a decision problem whose solution is a “yes” or “no” answer. An algorithm that solves all instances of a decision problem is said to be a polynomial-time algorithm if the time needed to find a solution to an arbitrary instance is $\mathcal{O}(n^k)$, where n is the size of the instance and k is a fixed positive integer. The computational complexity class P is composed of decision problems for which polynomial-time algorithms exist. Another important computational complexity class is the class NP which is composed of decision problems for which, for each such problem, a polynomial-time algorithm exists to verify the “yes” output of a candidate solution. The question of whether the classes P and NP are equal is one of the biggest open problems in theoretical computer science. It is widely conjectured that $P \neq NP$. A decision problem p is said to be polynomially transformable to a decision problem q if: (1) there exists a function f that maps every instance x of p into an instance $f(x)$ of q for which the answer to x is “yes” if and only if the answer to $f(x)$ is “yes”; and (2) a polynomial-time algorithm exists to compute $f(x)$ for every x in p . A problem is said to be NP -Complete if it belongs to NP and every problem in NP is polynomially transformable to it. Thus, if a polynomial-time algorithm is found for an NP -Complete problem, it follows that $P = NP$. In light of Shor's polynomial-time quantum factoring algorithm [2], Bennett et. al. [3] asked whether a polynomial-time quantum algorithm might exist to solve an NP -Complete problem. In other words, they asked, “Can a quantum computer solve an NP -Complete problem in polynomial-time?” Should the answer to this question

prove to be “yes”, it is widely recognized that this would have profound consequences for theoretical computer science [4].

In 2001, Farhi et. al. [5] examined the question of whether a quantum computer might be able to solve an NP -Complete problem in polynomial-time. They applied the quantum adiabatic search (QuAdS) algorithm introduced in Ref. [6] to find solutions of randomly generated hard instances of the NP -Complete problem N -Bit Exact Cover 3 which they believe to be classically intractable for sufficiently large inputs. The algorithm was simulated numerically on an existing (classical) computer. Because a quantum computer cannot be simulated efficiently on a classical computer, the simulations were restricted to $7 \leq N \leq 20$. They found that the median run-time $\overline{T}(N)$ for QuAdS to succeed on this class of instances could be fit with a quadratic scaling relation in the number of bits N (problem-size): $\overline{T}(N) \sim N^2$. It was pointed out that should classical algorithms truly require exponential time on this class of instances, and should the quadratic scaling behavior of QuAdS persist to large N , then QUAdS could outperform classical algorithms on randomly generated hard instances, though not necessarily on worst case instances. Their work has drawn a great deal of interest and suggests two possible directions for further research: (1) examining the large N scaling behavior of QuAdS; and (2) examining the robustness of QuAdS to noise. Recent progress on (1) appears in the work of Roland and Cerf [7]; Mitchell et. al. [8]; and Latorre and Orús [9, 10]. In this paper we will focus on the question of robustness of QuAdS to noise.

The analysis of Ref. [5] assumed that the quantum computer was perfectly isolated from noise. Childs et. al. [11] were the first to consider the robustness of QuAdS to noise. They presented numerical simulation results which suggested QuAdS might have an inherent robustness to

two types of noise-induced errors: (1) transitions out of the instantaneous ground state; and (2) unitary control errors. Their simulation did not, however, attempt to match the scale of the simulation presented in Ref. [5]. Recently, Roland and Cerf carried out an analytical study of QuAdS in the presence of noise using random matrix theory [12]. They showed that the error probability of QuAdS would not increase with problem-size N if the noise varies either very slowly or very rapidly with respect to the natural time-scale of the quantum computation \hbar/\overline{E} , where \overline{E} is the energy scale for the eigenvalues of the instantaneous Hamiltonian $H(t)$. Their analysis assumed weak noise which justified a perturbative analysis of their model.

As stated above, in this paper we will also examine the robustness of QuAdS to noise. Our work complements the analysis of Ref. [12] in that we consider noise that varies on a time-scale comparable to \hbar/\overline{E} . We extend the simulation protocol of Farhi et. al. [5] to include noise, and determine the noise-averaged median runtime $\langle T(N) \rangle$ for QuAdS to succeed on randomly generated instances of N-Bit Exact Cover 3 which have a unique solution. We find clear evidence of the sensitivity of QuAdS to noise. Two fits to the simulation results were carried out: (1) power-law scaling $\langle T(N) \rangle = aN^b$; and (2) exponential scaling $\langle T(N) \rangle = a[\exp(bN) - 1]$. Both types of scaling relations provided excellent fits, although the scaling parameters a and b varied with noise power, and with the noise polarization (defined in Section III A). Although we did encounter examples of noise realizations that reduce the runtime for QuAdS to succeed, at the largest noise power levels that we examined, the predominant effect of noise was to slowdown QuAdS. The sensitivity of QuAdS to noise polarization allows, for the first time, a determination of which noise polarizations are most problematic for QuAdS.

The structure of this paper is as follows. In section II we briefly describe the NP -Complete problem N-Bit Exact Cover 3, and review how QuAdS can be used to find a solution to an instance of this problem. In section III we describe our noise model and explain our extension of the simulation protocol of Farhi et. al. to include noise. In section IV we present the results of our simulation, and discuss their significance in section V. Section V also demonstrates how noise-induced dephasing leads to decoherence in QuAdS, estimates the amount of decoherence present in our simulations, and derives an upper bound for the noise-averaged QuAdS success probability in the weak noise limit that is appropriate for our simulations. Finally, in section VI, we provide a summary of our work.

II. EXACT COVER 3 AND QUANTUM ADIABATIC SEARCH

In this section we: (i) present the NP -Complete problem Exact Cover 3 (section II A); (ii) describe the quan-

tum adiabatic search algorithm and how it is used to solve instances of Exact Cover 3 (section II B); and (iii) describe the simulation protocol of Ref. [5] (section II C).

A. Exact Cover 3

Consider a collection of N binary variables (bits) z_1, \dots, z_N each of which can take on the value 0 or 1. The state of this N -bit system is specified by assigning values to each bit in the string $z = z_1 \dots z_N$. A total of 2^N states z are possible.

A specific instance of Exact Cover 3 (EC3) is composed of L clauses, each of which imposes a constraint on the values of three of the N bits. The number of clauses L will generally vary from one EC3-instance to another. If the i -th clause involves the bits $(a(i), b(i), c(i))$, then a particular bit-string $z = z_1 \dots z_N$ satisfies the clause if $z_{a(i)} + z_{b(i)} + z_{c(i)} = 1$. Otherwise, one says that z does not satisfy the clause. A bit-string z is said to solve an instance of EC3 if it satisfies all the clauses that make up the instance. If one is given an instance of EC3 and a candidate solution string z^* , one can check whether z^* solves the instance in polynomial-time since checking each of the L clauses simply requires adding three integers, and this can be done in polynomial-time. Thus EC3 belongs to NP . It can be shown that all problems in NP are polynomially transformable to EC3 [13] so that EC3 is also NP -Complete.

B. QuAdS and EC3

By combining the dynamics of the quantum adiabatic theorem with a clever choice of Hamiltonian $H(t)$, quantum adiabatic search (QuAdS) causes the state of a quantum computer (QC) to home-in on a solution of an instance of an NP -Complete problem [5]. We assume the NP -Complete problem is EC3. The quantum adiabatic theorem [14] assures us that if the initial state of a quantum system is the groundstate $|E_g(0)\rangle$ of the initial Hamiltonian $H(0)$, and $H(t)$ varies sufficiently slowly, then the quantum state at time T can be brought arbitrarily close to the groundstate of $H(T)$: $|\psi(T)\rangle = |E_g(T)\rangle + |\delta\psi\rangle$. The probability not to be in the groundstate, $\epsilon(T) = |\langle \delta\psi | \delta\psi \rangle|^2$, vanishes as $T \rightarrow \infty$. For a given instance of EC3, QuAdS evolves the state $|\psi(t)\rangle$ over a time interval $0 \leq t \leq T$, and the final Hamiltonian $H(T) = H_p$ is constructed so that its groundstate encodes a solution of the given instance. The initial Hamiltonian $H(0) = H_i$ is chosen so that its groundstate is non-degenerate and can be easily constructed, and $H(t)$ smoothly morphs $H_i \rightarrow H_p$:

$$H(t) = \left(1 - \frac{t}{T}\right) H_i + \left(\frac{t}{T}\right) H_p \quad . \quad (1)$$

We now briefly describe how H_i and H_p are constructed for a given instance of EC3.

Suppose that we are given an instance of N -bit EC3 composed of L clauses $C_i = (a(i), b(i), c(i))$ with $i = 1, \dots, L$, and that the bit-string $s = s_1 \dots s_N$ is a solution of this instance. Our QC is assumed to contain N qubits and the computational basis states $|z_1 \dots z_N\rangle$ are chosen to be eigenstates of $\sigma_z^1 \otimes \dots \otimes \sigma_z^N$. Although the QuAdS algorithm can be formulated more abstractly, it proves convenient to adopt the language of NMR. H_i , then, describes the Zeeman coupling of the qubits to an external magnetic field which points along the x -direction. The strength of the magnetic field at the site of the i -th qubit is equal to the number of clauses in the EC3 instance that contain bit i . The non-degenerate groundstate of H_i thus has all qubit spins aligned along \hat{x} so that $|E_g(0)\rangle$ is simply the uniform superposition of all 2^N computational basis states $|z_1 \dots z_N\rangle$. The final Hamiltonian H_p is constructed to be diagonal in the computational basis $|z_1 \dots z_N\rangle$:

$$H_p |z_1 \dots z_N\rangle = h(z_1, \dots, z_N) |z_1 \dots z_N\rangle . \quad (2)$$

The eigenvalue $h(z_1, \dots, z_N)$ is the sum of energy functions $h_{C_i}(z_{a(i)}, z_{b(i)}, z_{c(i)})$,

$$h(z_1, \dots, z_N) = \sum_{i=1}^L h_{C_i}(z_{a(i)}, z_{b(i)}, z_{c(i)}) , \quad (3)$$

where $C_i = (a(i), b(i), c(i))$ is the i -th clause in the given EC3 instance and,

$$h_{C_i}(z_{a(i)}, z_{b(i)}, z_{c(i)}) = \begin{cases} 0 & \text{if } z_1 \dots z_N \text{ satisfies } C_i \\ 1 & \text{otherwise} . \end{cases}$$

Thus $h(z_1, \dots, z_N)$ indicates how many clauses are violated by the string $z = z_1 \dots z_N$. All strings $s = s_1 \dots s_N$ that solve the given instance correspond to computational basis states $|s_1 \dots s_N\rangle$ that have zero energy, and which together span the groundstate eigenspace of H_p . EC3 instances which have a unique solution are referred to as unique satisfying assignment (USA) instances, and are believed to be the most difficult for QuAdS. In essence, it's harder to find a needle in a haystack that contains only one needle, than it is to find one in a haystack that contains many needles. For further discussion of instances with multiple satisfying assignments, see Ref. [15].

Thus, if our QC is initially prepared in the groundstate of H_i , and T is chosen to be sufficiently large that $H(t)$ evolves adiabatically, then the final state $|\psi(T)\rangle$ will lie in the groundstate eigenspace of H_p with probability $1 - \epsilon(T)$, where $\epsilon(T) = |\langle \delta\psi | \delta\psi \rangle|^2 \ll 1$. For a USA instance with solution string $s = s_1 \dots s_N$, measuring $|\psi(T)\rangle$ in the computational basis will give the solution string s with probability $1 - \epsilon(T)$. Let the string $z_1 \dots z_N$ be the actual measurement result. It can be quickly tested to determine whether it solves the USA instance. If "yes", the algorithm has succeeded, and $z = s$. If "no", then the quantum adiabatic search procedure is repeated until

the measurement result $z = s$. The algorithm's failure probability $\epsilon(T)$ will be much less than 1 if [14]:

$$T \gg \frac{\epsilon}{\Delta^2} , \quad (4)$$

where,

$$\epsilon = \max_{t \in [0, T]} \left| \langle E_1(t) | T \frac{dH}{dt} | E_g(t) \rangle \right| ; \quad (5)$$

$$\Delta = \min_{t \in [0, T]} |E_1(t) - E_g(t)| ; \quad (6)$$

and $|E_g(t)\rangle$ ($|E_1(t)\rangle$) is the groundstate (first excited state) of $H(t)$.

C. Noiseless Simulation Protocol

Farhi and co-workers [5, 6] studied the performance of QuAdS by numerically integrating the Schrodinger equation using $H(t)$ (eqn. (1)) to drive the dynamics. Because the Hilbert space for N -qubits has dimension 2^N , numerical simulation quickly becomes impractical since the number of wavefunction components that must be tracked by the numerical integration grows exponentially with N . This practical difficulty caused the simulations done in Refs. [5, 6] to be restricted to the range $7 \leq N \leq 20$. Only randomly generated USA instances were simulated as these authors believed that this set would provide hard cases for QuAdS, though not necessarily the worst cases.

An N -bit USA instance of EC3 is generated by the following procedure. The first clause is generated by picking 3 distinct integers in the range $[1, N]$ at random (uniform deviate). A count of the number of bit-strings of length N that satisfy the clause is then done. Distinct clauses continue to be generated in this manner, and with each new clause generated, a new count of the number of bit-strings that satisfy all clauses generated to that point is done. Eventually, the point is reached where enough clauses have been generated so that one of two situations occurs. (1) Only one bit-string s of length N remains that satisfies all the clauses generated. The collection of clauses then corresponds to an EC3-instance which has a unique solution s , and the procedure has thus produced a USA instance of EC3. (2) Addition of the most recently generated clause causes the set of all clauses produced to have no satisfying assignment (i. e. an EC3-instance has been produced with no solution). In this case, the instance is discarded and the above procedure is repeated until a USA instance is generated. The USA instance produced is then used to construct H_i and H_p , and from them, $H(t)$. The USA instances generated by this procedure were found to contain approximately as many clauses L as number of bits N : $L \sim N$.

In the adiabatic limit, $T \rightarrow \infty$, the QuAdS success probability $P_s \rightarrow 1$. Numerical simulations must necessarily work with finite T so that a protocol is needed to determine how to pick T . Farhi et. al. carried out

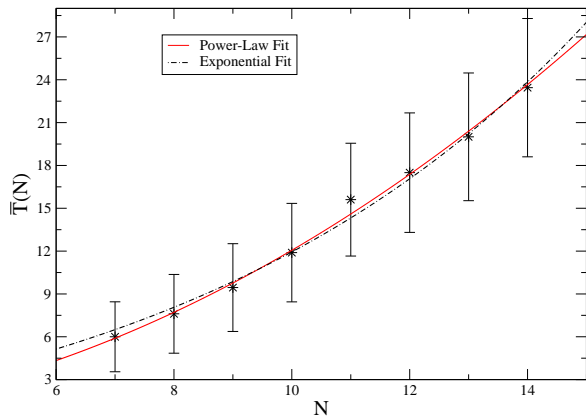


FIG. 1: Simulation results generated by our QuAdS numerical code for the noiseless median runtime $\bar{T}(N)$ (dimensionless units) versus the number of bits N . The solid line is the best power-law fit to the data and the dash-dot line is the best exponential fit. Respective values for a and b are given in the text. The error bars give 95% confidence limits for each median. Each datapoint is the outcome of averaging over 75 USA instances.

a hunting procedure which searches for a T that causes the simulation to produce a success probability P_s in the range $[0.12, 0.13]$. This corresponds to a success probability in the vicinity of $P_s = 0.125 = 1/2^3$. As noted in Ref. [5], this value of P_s is somewhat arbitrary, although for the values of N used in the simulations, it is much larger than $1/2^N$ which is the probability of the solution string s in the initial state. For each value of N , 75 USA instances are generated and QuAdS is used to find the solution to each instance. This generates runtimes $T_i(N)$ ($i = 1, \dots, 75$) from which the median runtime $\bar{T}(N)$ is determined. Farhi et. al. [5, 6] found that their simulation results for $\bar{T}(N)$ could be fit with a quadratic scaling relation for the range of N -values considered: $\bar{T}(N) \sim N^2$.

As a check on the soundness of our own simulation code, we repeated the noiseless calculation of Farhi et. al. for $7 \leq N \leq 14$. Figure 1 shows our results for $\bar{T}(N)$ versus N , together with a power-law fit to the simulation data: $\bar{T}(N) = aN^b$. The best-fit parameters are $a = 0.11966$ and $b = 2.0034$. The χ^2 value for the fit is 0.092, and the probability $P(\chi^2 \geq 0.092) = 0.9999844$. As noted in Section IV, the closer this probability is to 1, the more consistent the data-set is with the fitting function. We see that a power-law fit provides excellent agreement with our simulation results, and our exponent $b = 2.0034$ is consistent with the quadratic fit of Ref. [5]. Figure 1 also includes an exponential fit to the noiseless data. The best-fit parameters are: $a = 3.89566$; $b = 0.140235$; $\chi^2_{fit} = 0.214$; and $P(\chi^2 > 0.214) = 0.9998121$. We see that exponential scaling also provides an excellent fit to the data. We will comment further on this in Sections IV and V. The addition of noise to the simulation of QuAdS causes simulation to become impractical when $N \gtrsim 12$. In a couple of cases we were able to simulate

$N = 13$ and 14 (see Section IV). Our noiseless simulation will be used as a baseline for our simulation of QuAdS in the presence of noise. Since the simulations with noise do not go beyond $N = 14$, we did not extend the noiseless simulations beyond $N = 14$.

III. NOISY QUANTUM ADIABATIC SEARCH

In this section we discuss QuAdS in the presence of noise. Section III A presents our noise model and describes how noise realizations are constructed. Section III B discusses how the noiseless simulation protocol is modified to allow a study of the noise-averaged performance of QuAdS.

A. Noise Model

We consider noise $\mathbf{N}_i(t)$ that couples to the qubits via the Zeeman interaction:

$$H_{int} = - \sum_{i=1}^N \gamma_i \boldsymbol{\sigma}_i \cdot \mathbf{N}_i(t) . \quad (7)$$

The qubits are labeled by the index i and the subscript i on the noise field $\mathbf{N}_i(t)$ and coupling constant γ_i indicates that they can vary from one qubit site to another. We assume the noise is a stationary random process. To simplify the presentation of our noise model we initially consider a one-component noise field $N(t)$. The presentation is easily generalized to three-component spatially varying noise $\mathbf{N}_i(t)$.

The rate at which the noise field $N(t)$ can do work (i. e. noise power) is [16],

$$P = N^2(t) ,$$

and the energy that can be delivered in a time interval dt is,

$$dE = N^2(t) dt .$$

We consider power-type noise for which the time-averaged noise power

$$\bar{P} = \lim_{T \rightarrow \infty} \frac{1}{T} \int_{-T/2}^{T/2} N^2(t) dt \quad (8)$$

is finite. The total noise energy

$$E = \int_{-\infty}^{\infty} dt N^2(t) \quad (9)$$

diverges for this class of noise. The divergence is due to the occurrence of an infinite number of noise fluctuations in the time interval $-\infty < t < \infty$. The energy of an individual fluctuation is, however, finite.

The mean noise power \overline{P} can be related to the noise correlation function,

$$\overline{N(t)N(t-s)} \equiv \lim_{T \rightarrow \infty} \frac{1}{T} \int_{-T/2}^{T/2} dy N(y)N(y-s) . \quad (10)$$

Comparing eqns. (8) and (10) we see that,

$$\overline{P} = \overline{N^2(t)} . \quad (11)$$

The Weiner-Khintchine theorem [17] shows that the noise correlation function and the power spectral density $S_N(f)$ form a Fourier transform pair:

$$\overline{N(t)N(t-s)} = \int_{-\infty}^{\infty} df S_N(f) e^{-2\pi i f s} . \quad (12)$$

Thus, it follows from eqns. (11) and (12) that

$$\overline{P} = \int_{-\infty}^{\infty} df S_N(f) , \quad (13)$$

which identifies $S_N(f)$ as the mean noise power available in the frequency interval $(f, f + df)$.

Having reviewed these basic facts about stationary random processes, we are now in a position to describe our noise model and to write out the basic relations that are necessary to construct an individual realization of the noise.

The noise $N(t)$ is produced by a sequence of randomly occurring noise fluctuations $F(t)$. The fluctuations: (1) occur independently of each other at average rate \overline{n} per unit time; and (2) have a peak value x which is Gaussian distributed with mean $\overline{x} = 0$, variance $\overline{x^2} = \sigma^2$, and temporal width 2τ , where τ is the thermal relaxation time. The bandwidth of $F(t)$ is $\Delta\omega \sim 1/2\tau$. Thus,

$$N(t) = \sum_i F(t - t_i) ,$$

where i labels the noise fluctuations, and t_i specifies the center of the i th fluctuation. The mean number of fluctuations $\overline{N_f}$ occurring in the time interval $[0, T]$ is $\overline{N_f} = \overline{n}T$. It is well-known that for noise with these properties, the actual number of fluctuations n that occur in a time T is governed by the Poisson distribution [18]:

$$p(n) = \frac{(\overline{N_f})^n}{n!} e^{-\overline{N_f}} .$$

The energy present in a single fluctuation is:

$$\varepsilon = \int_{-\infty}^{\infty} F^2(t) dt . \quad (14)$$

Let $F(t) = x h(t)$, where $h(t)$ is any convenient function of finite support with normalization

$$\int_{-\infty}^{\infty} dt h^2(t) = 2\tau .$$

As mentioned above, x is Gaussian distributed with mean $\overline{x} = 0$ and $\overline{x^2} = \sigma^2$. From eqn. (14), $\varepsilon = 2x^2\tau$, and the mean energy per fluctuation $\overline{\varepsilon}$ is,

$$\overline{\varepsilon} = 2\overline{x^2}\tau = 2\sigma^2\tau . \quad (15)$$

From Campbell's theorem [19], the power spectral density for $N(t)$ is

$$S_N(f) = \overline{n} |g(f)|^2 , \quad (16)$$

where $g(f)$ is the Fourier transform of the fluctuation profile $F(t)$. Thus, using eqns. (13), (16), and Paresval's theorem gives,

$$\overline{P} = \overline{n} \int_{-\infty}^{\infty} dt F^2(t) . \quad (17)$$

Finally, using eqns. (14) and (15) gives,

$$\overline{P} = 2\overline{n}\sigma^2\tau . \quad (18)$$

Thus we see that our noise model is characterized by any 3 of the parameters \overline{P} , \overline{n} , σ^2 , and τ .

The numerical simulation constructs a realization of the noise as follows. We sample a positive integer N_f according to the Poisson distribution with mean $\overline{N_f} = \overline{n}T$, where T is the duration of the search. N_f is the number of fluctuations present in the noise realization. The noise model assumes these fluctuations occur independently with probability $dp_f = (1/T)dt$. We sample N_f numbers t_i ($i = 1, \dots, N_f$) from the interval $(0, T)$. The t_i correspond to the temporal centers of the N_f fluctuations. For simplicity, we've assumed that the fluctuation profile $h(t)$ is a square pulse. We next carry out N_f samples x_i ($i = 1, \dots, N_f$) of a Gaussian distribution with mean $\overline{x_i} = 0$ and variance $\overline{x_i^2} = \sigma^2$. Here x_i is the peak value of the i -th fluctuation. These sample results produce the noise realization $N(t)$:

$$N(t) = \sum_{i=1}^{N_f} x_i \left[\frac{\text{sgn}(t - t_{il}) - \text{sgn}(t - t_{ir})}{2} \right] , \quad (19)$$

where $t_{il} = t_i - \tau$, and $t_{ir} = t_i + \tau$. We shall need to produce noise realizations with arbitrary mean noise power \overline{P} . We do this by the following normalization procedure. First we calculate the mean noise power \overline{P} of the noise realization $N(t)$ just produced:

$$\overline{P} = \frac{1}{T} \int_0^T dt N^2(t) . \quad (20)$$

Then, if the desired value for the noise power is \overline{P} , we rescale $N(t)$ in eqn. (19) so that $N(t) \rightarrow n(t) \equiv \sqrt{\overline{P}/\overline{P}} N(t)$. The result is a noise realization $n(t)$ with mean noise power \overline{P} . The simulation takes as inputs the mean noise power \overline{P} , the variance $\overline{x_i^2} = \sigma^2$, and the thermal relaxation time τ . The fluctuation rate \overline{n} then

follows from eqn. (18): $\bar{n} = \bar{P}/(2\sigma^2\tau)$. This procedure is used to produce 4 types of noise that are characterized by the polarization, or direction along which the noise $\mathbf{N}_i(t)$ fluctuates: (i) \hat{x} ; (ii) \hat{y} ; (iii) \hat{z} ; and (iv) all 3 directions simultaneously. We shall refer to these noise polarization types as x-type; y-type; z-type; and 3-type noise, respectively. The noise $\mathbf{N}_i(t)$ is then introduced into eqn. (7) and the full Hamiltonian $\mathcal{H}(t)$ is the sum of $H(t)$ (eqn. (1)) and $H_{int}(t)$ (eqn. (7)):

$$\mathcal{H}(t) = H(t) + H_{int}(t) . \quad (21)$$

$\mathcal{H}(t)$ drives the Schrodinger dynamics of QuAdS in the presence of the noise realization $\mathbf{N}_i(t)$. We now go on to explain how the noiseless simulation protocol of Ref. [5] is extended to include the effects of noise.

B. Noisy Simulation Protocol

We would like to compare how the 4 different noise types introduced above impact the performance of QuAdS. To that end, we determine the scaling relation for the noise-averaged median runtime $\langle T(N) \rangle$ versus N for each type of noise. Just as in the noiseless protocol, for each value of N , we generate 75 USA instances of EC3. QuAdS, in the presence of each of the 4 noise types, is then applied to the *same* 75 USA instances. This allows an apples-to-apples comparison of how the different noise types affect QuAdS performance. For each noise type, and each USA instance, we generate 10 noise realizations and use the Hamiltonian $\mathcal{H}(t)$ to find the 10 corresponding QuAdS runtimes $T_i^j(N)$. Here j labels the noise realizations ($j = 1, \dots, 10$), and i labels the USA instances ($i = 1, \dots, 75$). Thus, for each value of N , and each noise type, 750 runtimes are found. The ensemble \mathcal{E}_N of 750 runtimes $T_i^j(N)$ allows us to estimate the statistical effects of each noise type on QuAdS performance over the full set of 75 USA instances. The noise-averaged median runtime $\langle T(N) \rangle$ is then identified with the median runtime calculated from the noise ensemble \mathcal{E}_N . We then fit the simulation results using both power-law scaling $\langle T(N) \rangle = aN^b$ and exponential scaling $\langle T(N) \rangle = a[\exp(bN) - 1]$, and calculated the χ^2 for each type of fit. We determine 2 such fits for each of the 4 noise types. For each fit-type, we compared the respective scaling exponents to get a quantitative measure of which of the 4 noise types most adversely affects QuAdS. As will be discussed in Section IV, scaling curves will be determined for each of the 4 noise types for 3 different noise power levels. As pointed out at the end of Section II C, most simulations will be restricted to $7 \leq N \leq 12$, though for x-type noise, the upper limit could be extended to $N = 13$ and 14. It is important to recognize that each point on a given scaling curve is based on 750 runtimes, and so each scaling curve with $7 \leq N \leq 12$ ($7 \leq N \leq 14$) is distilled from 4500 (6000) runtimes. Each runtime $T_i^j(N)$ is itself the result of a

hunting procedure that requires, on average, 5 integrations of the Schrodinger equation. Thus a single scaling curve corresponds to approximately 22,500 (30,000) integrations of the Schrodinger equation. As mentioned above, we generate 4 such curves for each noise power level, and we present data for 3 power levels. Putting all this together, we see that the simulation results we present in this paper are the outcome of approximately 300,000 integrations of the Schrodinger equation. This work was done, initially on our own 16-node Beowulf cluster, and later on the TeraGrid cluster which was accessed through the National Center for Supercomputing Applications (NCSA) in Urbana, Illinois.

IV. SIMULATION RESULTS

In this Section we present our simulation results for noisy QuAdS. The noise model parameters (see Section III) were chosen to be $\sigma = 0.2$; $\tau = 1$; and $\bar{P} = 0.001, 0.003, 0.005$. This produced noise that was strong enough to affect QuAdS performance, though not so strong as to make large-scale simulation impractical. Both H_i and H_p have energy-level spacing $\Delta E \sim 1$. For our choice of τ , $\Delta E \sim 2/\tau$, so that our noise bandwidth matches the natural resonance energies of the quantum computer. We are thus probing QuAdS in a noise regime that complements that studied in Ref. [12]. Further discussion of our choice of noise parameters will be given in Section V. As this was our first large-scale simulation of noisy QuAdS, we decided to simplify the noise model by restricting the noise field and coupling constants to be the same for each qubit: $\mathbf{N}_i(t) = \mathbf{N}(t)$ and $\gamma_i = 1$. We plan to lift this restriction in our next set of simulations. We also plan to parallelize the hunting procedure which should substantially speed up the code, allowing us to explore larger values of mean noise power \bar{P} . To get a sense of how long the following simulation took in real time, note that producing one scaling curve at $\bar{P} = 0.005$ took approximately 3 weeks on our 16-node Beowulf cluster. The same simulation took approximately 72–96 hours on the TeraGrid cluster at NCSA.

We now present our simulation results. For each mean noise power \bar{P} we present 4 figures and 2 tables. Each of the figures contains our numerical results for $\langle T(N) \rangle$ for a particular noise polarization type (x, y, z, 3), along with two fits to the data: (i) a power-law fit $\langle T(N) \rangle = aN^b$; and (ii) an exponential fit $\langle T(N) \rangle = a[\exp(bN) - 1]$. Information about the best fits to the data are collected in the two tables, one table for each of the fitting functions. Each table contains: (i) the best fit parameters; (ii) the chi-squared for the fit χ_{fit}^2 ; and (iii) the probability $P(\chi^2 > \chi_{fit}^2)$ that, assuming the fitting function correctly describes the scaling of $\langle T(N) \rangle$ versus N , a sampling of $\langle T(N) \rangle$ would yield a $\chi^2 > \chi_{fit}^2$. The closer this probability is to 1, the more consistent the data-set is with the fitting function. As such, it provides a quantitative measure of the quality of fit to the data. Note

that, due to the finite-size of the data-set, more than one fitting function can be consistent with the data. To help the reader locate specific results, we provide the following roadmap through the figures and tables.

1. Figures 2, 3, 4, and 5 correspond to x, y, z, and 3-type noise with $\bar{P} = 0.001$, respectively. Tables I and II give the specifics of the power-law and exponential fits through these data-sets, respectively. Table entries are ordered according to increasing scaling-exponent b .
2. Figures 6, 7, 8, and 9 correspond to x, y, z, and 3-type noise with $\bar{P} = 0.003$, respectively. Tables III and IV give the specifics of the power-law and exponential fits through these data-sets, respectively. Table entries are ordered according to increasing scaling-exponent b .
3. Figures 10, 11, 12, and 13 correspond to x, y, z, and 3-type noise with $\bar{P} = 0.005$, respectively. Tables V and VI give the specifics of the power-law and exponential fits through these data-sets, respectively. Table entries are ordered according to increasing scaling-exponent b .

Examination of these figures and tables shows that the power-law and exponential fits *both* provide excellent fits to the numerical results. One sees that the probability $P(\chi^2 > \chi_{fit}^2)$, and hence the quality of fit, shows a slight decrease with increasing mean noise power \bar{P} , and that the rate of decrease in the fit quality is largest for y-type noise. One also notes that the quality of the exponential fit decreases *more slowly* than does the quality of the power-law fit. Further discussion of these results is given in Section V.

TABLE I: Summary of best-fit parameters for power-law scaling curves for $\bar{P} = 0.001$. For comparison, best-fit parameters for noiseless QuAdS are also included.

\bar{P}	noise type	a	b	χ_{fit}^2	$P(\chi^2 > \chi_{fit}^2)$
0.000	—	1.1966×10^{-1}	2.0034	0.092	0.9999844
0.001	x	1.1447×10^{-1}	2.0267	0.083	0.9999886
0.001	3	1.0635×10^{-1}	2.0594	0.064	0.9994915
0.001	z	1.0395×10^{-1}	2.0695	0.063	0.9995085
0.001	y	9.6766×10^{-2}	2.1075	0.078	0.9992617

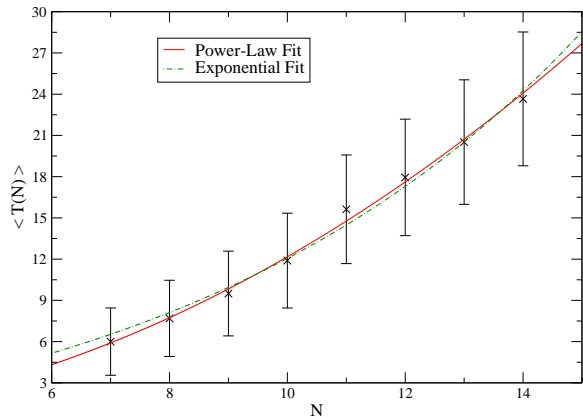


FIG. 2: Simulation results for QuAdS with noise polarized along \hat{x} and mean noise power $\bar{P} = 0.001$. Plotted are the noise-averaged median runtime $\langle T(N) \rangle$ (dimensionless units) versus the number of bits N . The solid line is the best power-law fit to the data and the dash-dot line is the best exponential fit to the data. The error bars give 95% confidence limits for each median. Each datapoint is the outcome of averaging over 75 USA instances and 10 noise realizations per USA instance.

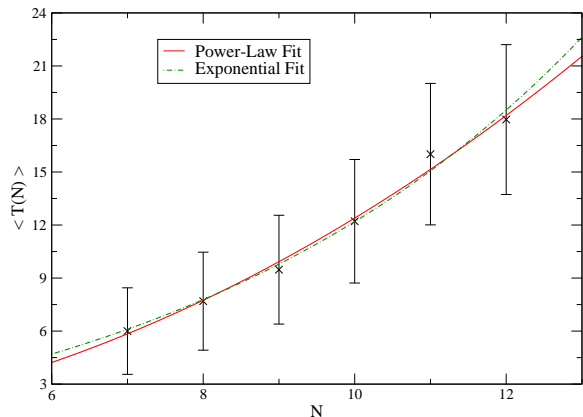


FIG. 3: Simulation results for QuAdS with noise polarized along \hat{y} and mean noise power $\bar{P} = 0.001$. Plotted are the noise-averaged median runtime $\langle T(N) \rangle$ (dimensionless units) versus the number of bits N . The solid line is the best power-law fit to the data and the dash-dot line is the best exponential fit to the data. The error bars give 95% confidence limits for each median. Each datapoint is the outcome of averaging over 75 USA instances and 10 noise realizations per USA instance.

V. DISCUSSION

A. Summary

We examine here what can be learned from the results presented in Section IV. To begin, we note that both power-law scaling $\langle T(N) \rangle = aN^b$ and exponential scaling $\langle T(N) \rangle = a[\exp(bN) - 1]$ provide excellent fits

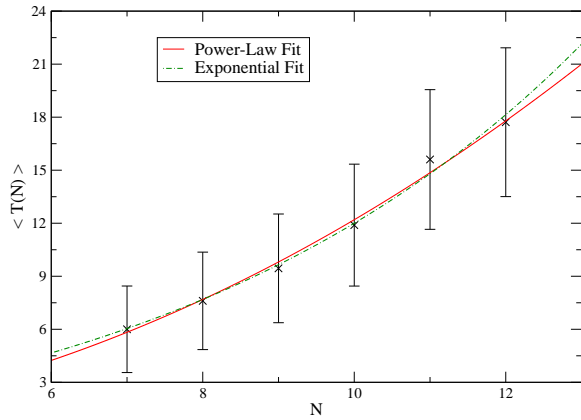


FIG. 4: Simulation results for QuAdS with noise polarized along \hat{z} and mean noise power $\bar{P} = 0.001$. Plotted are the noise-averaged median runtime $\langle T(N) \rangle$ (dimensionless units) versus the number of bits N . The solid line is the best power-law fit to the data and the dash-dot line is the best exponential fit to the data. The error bars give 95% confidence limits for each median. Each datapoint is the outcome of averaging over

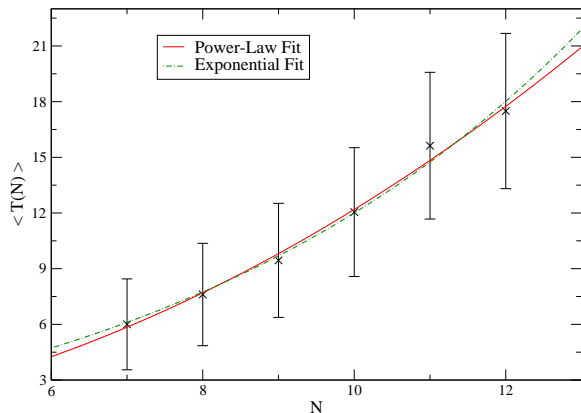


FIG. 5: Simulation results for QuAdS with noise polarization along all 3 directions and mean noise power $\bar{P} = 0.001$. Plotted are the noise-averaged median runtime $\langle T(N) \rangle$ (dimensionless units) versus the number of bits N . The solid line is the best power-law fit to the data and the dash-dot line is the best exponential fit to the data. The error bars give 95% confidence limits for each median. Each datapoint is the outcome of averaging over 75 USA instances and 10 noise realizations per USA instance.

to our simulation results, although the fit parameters are noise dependent. Tables I–VI show that the scaling exponent b increases with increasing mean noise power \bar{P} , and the rate at which it increases depends on the noise polarization, or direction along which the noise field $\mathbf{N}_i(t)$ fluctuates. Clearly, as the scaling exponent increases, QuAdS performance decreases non-linearly. We simulated noise with noise polarization: (i) along \hat{x} ; (ii) along

TABLE II: Summary of best-fit parameters for exponential scaling curves for $\bar{P} = 0.001$.

\bar{P}	noise type	a	b	χ^2_{fit}	$P(\chi^2 > \chi^2_{fit})$
0.001	x	3.81403	0.142561	0.216	0.9998065
0.001	3	2.60771	0.172331	0.075	0.9993111
0.001	z	2.46414	0.176985	0.059	0.9995798
0.001	y	2.42677	0.179578	0.085	0.9991179

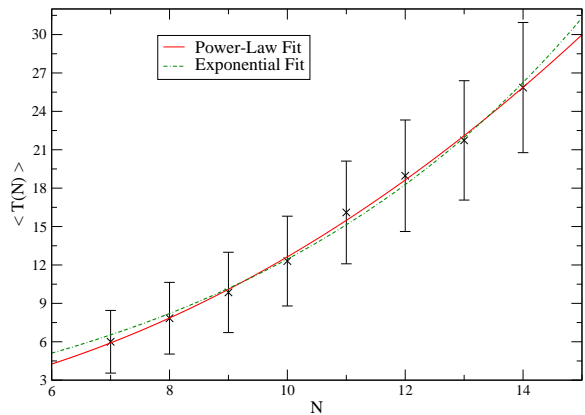


FIG. 6: Simulation results for QuAdS with noise polarized along \hat{x} and mean noise power $\bar{P} = 0.003$. Plotted are the noise-averaged median runtime $\langle T(N) \rangle$ (dimensionless units) versus the number of bits N . The solid line is the best power-law fit to the data and the dash-dot line is the best exponential fit to the data. The error bars give 95% confidence limits for each median. Each datapoint is the outcome of averaging over 75 USA instances and 10 noise realizations per USA instance.

\hat{y} ; (iii) along \hat{z} ; and (iv) along all 3 directions simultaneously. At the noise power levels considered, x-type noise was found to have the smallest impact on QuAdS performance, while y-type noise was found to cause the largest slowdown. As noted in Section IV, although the quality of both the power-law and exponential fits is excellent in all cases considered, we did see a slight reduction in the quality of fit as noise power increased for all noise-types except x-type noise. We also noted (see Tables V and VI especially) that the quality of the exponential fit decreased at a slightly slower rate than did the power-law fit. It would clearly be of interest to extend the simulations to larger noise power levels to examine: (i) how rapidly the scaling exponent b increases with noise power; and (ii) how quickly the quality of fit for both power-law and exponential fits deteriorates with increasing noise power. Given that a quantum computer will eventually crossover to classical behavior with sufficient noise power, and should classical algorithms truly require exponential time on the randomly generated hard instances considered in Ref. [5] and here, then one would anticipate a power-law fit to eventually become inconsis-

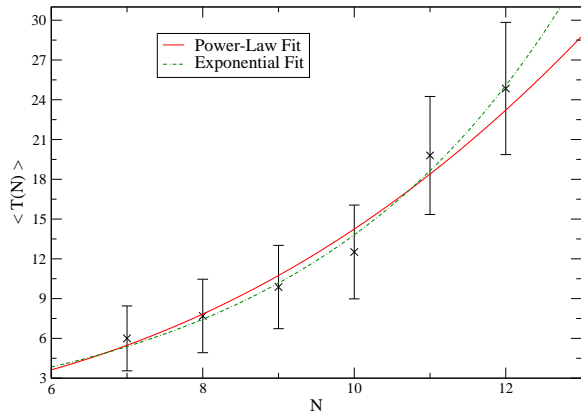


FIG. 7: Simulation results for QuAdS with noise polarized along \hat{y} and mean noise power $\bar{P} = 0.003$. Plotted are the noise-averaged median runtime $\langle T(N) \rangle$ (dimensionless units) versus the number of bits N . The solid line is the best power-law fit to the data and the dash-dot line is the best exponential fit to the data. The error bars give 95% confidence limits for each median. Each datapoint is the outcome of averaging over 75 USA instances and 10 noise realizations per USA instance.

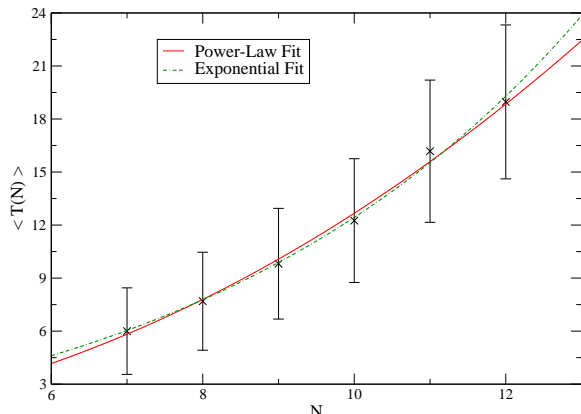


FIG. 8: Simulation results for QuAdS with noise polarized along \hat{z} and mean noise power $\bar{P} = 0.003$. Plotted are the noise-averaged median runtime $\langle T(N) \rangle$ (dimensionless units) versus the number of bits N . The solid line is the best power-law fit to the data and the dash-dot line is the best exponential fit to the data. The error bars give 95% confidence limits for each median. Each datapoint is the outcome of averaging over 75 USA instances and 10 noise realizations per USA instance.

tent with the simulation data at sufficient noise power and the exponential fit to provide the better fit. Beyond this threshold value of noise power, QuAdS would then be expected to have performance comparable with classical algorithms. Observation of such a crossover would be extremely important as it would give a direct measure of how much noise QuAdS can tolerate. In the following

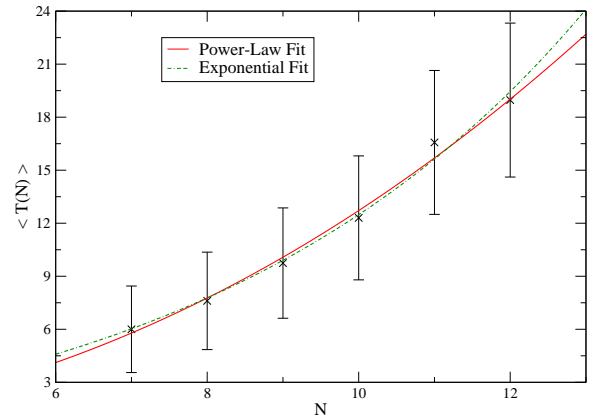


FIG. 9: Simulation results for QuAdS with noise polarization along all 3 directions and mean noise power $\bar{P} = 0.003$. Plotted are the noise-averaged median runtime $\langle T(N) \rangle$ (dimensionless units) versus the number of bits N . The solid line is the best power-law fit to the data and the dash-dot line is the best exponential fit to the data. The error bars give 95% confidence limits for each median. Each datapoint is the outcome of averaging over 75 USA instances and 10 noise realizations per USA instance.

TABLE III: Summary of best-fit parameters for power-law scaling curves for $\bar{P} = 0.003$. For comparison, best-fit parameters for noiseless QuAdS are also included.

\bar{P}	noise type	a	b	χ^2_{fit}	$P(\chi^2 > \chi^2_{fit})$
0.000	—	1.1966×10^{-1}	2.0034	0.092	0.9999844
0.003	x	9.3604×10^{-2}	2.1304	0.052	0.9999971
0.003	z	8.4209×10^{-2}	2.1774	0.050	0.9996975
0.003	3	7.8825×10^{-2}	2.2077	0.083	0.9991666
0.003	y	2.9821×10^{-2}	2.6792	0.570	0.9663310

subsection we show that noise-induced dephasing leads to decoherence in QuAdS, estimate how much decoherence is present in our simulations, and derive an upper bound for the noise-averaged QuAdS success probability.

B. Noise-Induced Decoherence in QuAdS

Although our focus in this paper is on QuAdS, the following analysis can be adapted to the more general situation of noisy quantum adiabatic dynamics. We will report on this elsewhere.

The total Hamiltonian for noisy QuAdS is (see eq. (21)),

$$\mathcal{H}(t) = H(t) + H_{int}(t) \quad ,$$

with $H(t)$ and $H_{int}(t)$ given in eqs. (1) and (7), respectively. In the Schrodinger picture, the dynamics is driven

TABLE IV: Summary of best-fit parameters for exponential scaling curves for $\bar{P} = 0.003$.

\bar{P}	noise type	a	b	χ_{fit}^2	$P(\chi^2 > \chi_{fit}^2)$
0.003	x	3.24309	0.157716	0.169	0.9999056
0.003	z	2.10817	0.193125	0.036	0.9998428
0.003	3	2.05131	0.195818	0.075	0.9993165
0.003	y	0.847514	0.285049	0.283	0.9908794

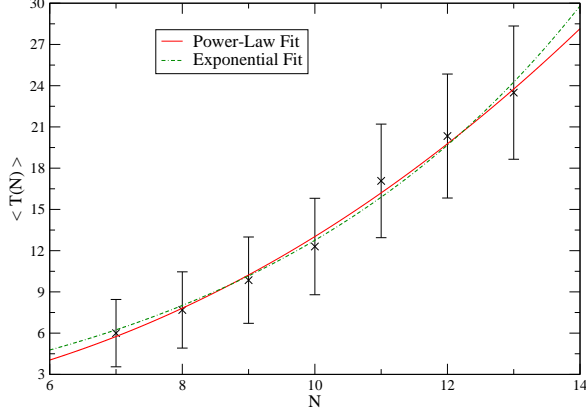


FIG. 10: Simulation results for QuAdS with noise polarized along \hat{x} and mean noise power $\bar{P} = 0.005$. Plotted are the noise-averaged median runtime $\langle T(N) \rangle$ (dimensionless units) versus the number of bits N . The solid line is the best power-law fit to the data and the dash-dot line is the best exponential fit to the data. The error bars give 95% confidence limits for each median. Each datapoint is the outcome of averaging over 75 USA instances and 10 noise realizations per USA instance.

by

$$i \frac{\partial}{\partial t} |\psi\rangle = \mathcal{H}(t) |\psi\rangle .$$

Transforming to an interaction-like picture (the time-ordering symbol is suppressed),

$$|\psi(t)\rangle = \exp \left[-i \int_0^t ds H_{int}(s) \right] |\chi(t)\rangle , \quad (22)$$

the equation of motion for $|\chi(t)\rangle$ is found to be

$$i \frac{\partial}{\partial t} |\chi\rangle = \bar{H}(t) |\chi\rangle , \quad (23)$$

where

$$\bar{H}(t) = e^{i \int_0^t ds H_{int}(s)} H(t) e^{-i \int_0^t ds H_{int}(s)} . \quad (24)$$

Using the well-known identity

$$e^{\xi A} B e^{-\xi A} = B + \xi [A, B] + \frac{\xi^2}{2} [A, [A, B]] + \dots \quad (25)$$

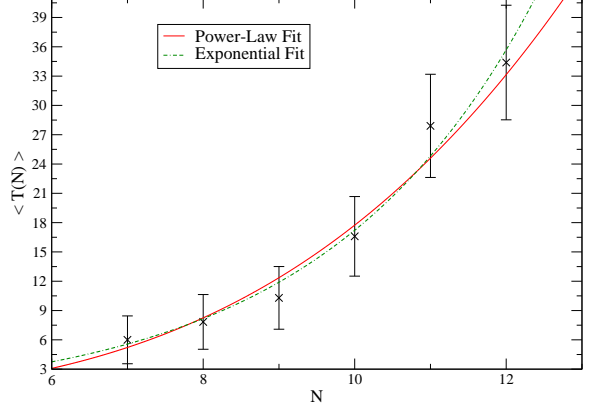


FIG. 11: Simulation results for QuAdS with noise polarized along \hat{y} and mean noise power $\bar{P} = 0.005$. Plotted are the noise-averaged median runtime $\langle T(N) \rangle$ (dimensionless units) versus the number of bits N . The solid line is the best power-law fit to the data and the dash-dot line is the best exponential fit to the data. The error bars give 95% confidence limits for each median. Each datapoint is the outcome of averaging over 75 USA instances and 10 noise realizations per USA instance.

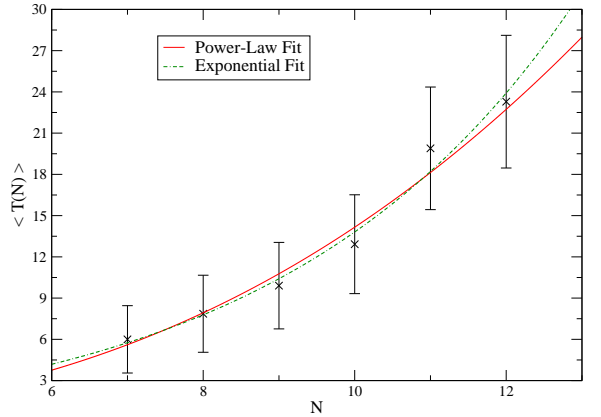


FIG. 12: Simulation results for QuAdS with noise polarized along \hat{z} and mean noise power $\bar{P} = 0.005$. Plotted are the noise-averaged median runtime $\langle T(N) \rangle$ (dimensionless units) versus the number of bits N . The solid line is the best power-law fit to the data and the dash-dot line is the best exponential fit to the data. The error bars give 95% confidence limits for each median. Each datapoint is the outcome of averaging over 75 USA instances and 10 noise realizations per USA instance.

with $B = H(t)$ and

$$\begin{aligned} \xi A &= i \int_0^t ds H_{int}(s) \\ &= \left[-i\gamma \int_0^t x(s) ds \right] \sum_{i=1}^N \sigma_x^i , \end{aligned} \quad (26)$$

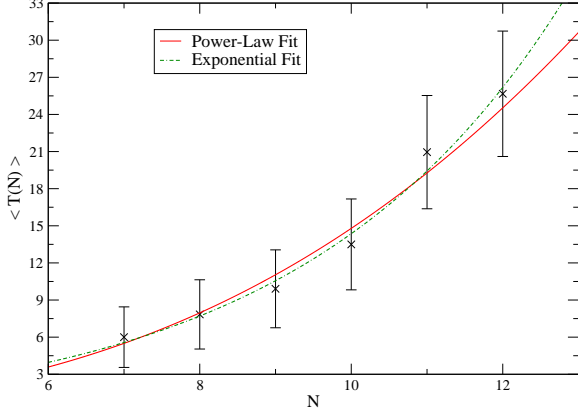


FIG. 13: Simulation results for QuAdS with noise polarization along all 3 directions and mean noise power $\bar{P} = 0.005$. Plotted are the noise-averaged median runtime $\langle T(N) \rangle$ (dimensionless units) versus the number of bits N . The solid line is the best power-law fit to the data and the dash-dot line is the best exponential fit to the data. The error bars give 95% confidence limits for each median. Each datapoint is the outcome of averaging over 75 USA instances and 10 noise realizations per USA instance.

TABLE V: Summary of best-fit parameters for power-law scaling curves for $\bar{P} = 0.005$. For comparison, best-fit parameters for noiseless QuAdS are also included.

\bar{P}	noise type	a	b	χ_{fit}^2	$P(\chi^2 > \chi_{fit}^2)$
0.000	—	1.1966×10^{-1}	2.0034	0.092	0.9999844
0.005	x	6.679×10^{-2}	2.2901	0.132	0.9996794
0.005	z	3.5862×10^{-2}	2.5964	0.389	0.9833500
0.005	3	2.4823×10^{-2}	2.7752	0.484	0.9750332
0.005	y	6.6069×10^{-3}	3.429	1.052	0.9017628

identifies

$$\xi = -i\gamma \int_0^t x(s) ds \quad , \quad (27)$$

and

$$A = \sum_{i=1}^N \sigma_x^i \quad . \quad (28)$$

To make our discussion concrete, I will assume the presence of x-noise: $\mathbf{N}_i(t) = x(t)\hat{\mathbf{x}}$; and set $\gamma_i = \gamma$. Combining eqs. (24) through (28) gives

$$\bar{H}(t) = H(t) - \left(i\gamma \int_0^t x(s) ds \right) \left[\sum_{i=1}^N \sigma_x^i, H(t) \right] + \dots \quad (29)$$

In the simplest approximation, only the first term in eq. (29) is kept. This corresponds to the limit of weak

TABLE VI: Summary of best-fit parameters for exponential scaling curves for $\bar{P} = 0.005$.

\bar{P}	noise type	a	b	χ_{fit}^2	$P(\chi^2 > \chi_{fit}^2)$
0.005	x	2.25018	0.189744	0.178	0.9993283
0.005	z	1.12768	0.258381	0.256	0.9924477
0.005	3	0.859322	0.287436	0.253	0.9926288
0.005	y	0.498037	0.357153	0.707	0.9504644

noise which is appropriate for our simulations. Clearly eq. (29) lends itself to a systematic evaluation of corrections to the weak noise approximation. Evaluating eq. (22) at the end of the quantum search $t = T$ gives

$$|\psi(T)\rangle = \exp \left[-i \int_0^T ds H_{int}(s) \right] |\chi(T)\rangle \quad , \quad (30)$$

and in the weak noise approximation, eq. (23) becomes

$$i \frac{\partial}{\partial t} |\chi\rangle = H(t) |\chi\rangle \quad . \quad (31)$$

Thus, in the weak noise limit, the time-development of $|\chi(t)\rangle$ is driven by the Hamiltonian $H(t)$ for noiseless QuAdS.

To evaluate eq. (30), we introduce the instantaneous eigenvalues and eigenstates of $H_{int}(t)$:

$$H_{int}(t) |E_{\sigma}(t)\rangle = E_{\sigma}(t) |E_{\sigma}(t)\rangle \quad . \quad (32)$$

Following the usual decoherence language [20], we refer to the $|E_{\sigma}(t)\rangle$ as the pointer basis states. For x-noise, the pointer basis states are time-independent:

$$\begin{aligned} |E_{\sigma}(t)\rangle &= |E_{\sigma}\rangle \\ &= |\sigma_1 \cdots \sigma_N\rangle_x \\ &= |\sigma_1\rangle_x \otimes \cdots \otimes |\sigma_N\rangle_x \quad , \end{aligned} \quad (33)$$

where $\sigma_i = \pm 1$ and $\sigma = (\sigma_1, \dots, \sigma_N)$. It follows from our expression for $H_{int}(t)$ (eqs. (7), (32), and (33)) that

$$E_{\sigma}(t) = -\gamma x(t) \sigma \quad , \quad (34)$$

with

$$\sigma = \sum_{i=1}^N \sigma_i \quad . \quad (35)$$

Dividing the time interval $[0, T]$ into N subintervals of duration $\epsilon = T/N$, and noting that $[H_{int}(t), H_{int}(t')] = 0$ for x-noise allows us to write the exponential in eq. (30) as

$$\exp \left[-i \int_0^T ds H_{int}(s) \right] = \prod_{i=1}^N U(t_i, t_{i-1}) \quad , \quad (36)$$

where

$$U(t_i, t_{i-1}) = \exp \left[-i \int_{t_{i-1}}^{t_i} ds H_{int}(s) \right] . \quad (37)$$

Using eq. (36) and inserting the completeness relation for the pointer basis states $\{ |E_\sigma\rangle \}$ into eq. (30) gives

$$|\psi(T)\rangle = \sum_{\sigma_1 \cdots \sigma_N} |\sigma_1 \cdots \sigma_N\rangle \langle \sigma_1 \cdots \sigma_N | \prod_{i=1}^N U(t_i, t_{i-1}) |\chi(T)\rangle . \quad (38)$$

Using eqs. (37) and (32) gives

$$\langle \sigma_1 \cdots \sigma_N | U(t_i, t_{i-1}) = \langle \sigma_1 \cdots \sigma_N | \exp \left[-i \int_{t_{i-1}}^{t_i} ds E_\sigma(s) \right] . \quad (39)$$

Finally, using eq. (39) in eq. (38) gives

$$|\psi(T)\rangle = \sum_{\sigma_1 \cdots \sigma_N} |\sigma_1 \cdots \sigma_N\rangle \exp[-i\phi_\sigma(T)] a_\sigma(T) , \quad (40)$$

where

$$\phi_\sigma(T) = \int_0^T ds E_\sigma(s) = -\gamma\sigma \int_0^T x(s) ds , \quad (41)$$

and

$$a_\sigma(T) = \langle \sigma_1 \cdots \sigma_N | \chi(T) \rangle . \quad (42)$$

The final density matrix $\rho(T) = |\psi(T)\rangle \langle \psi(T)|$ has matrix elements (in the pointer basis)

$$\rho_{\sigma, \sigma'}(T) = \exp[-i\Gamma_{\sigma, \sigma'}] a_\sigma(T) a_{\sigma'}^*(T) , \quad (43)$$

where

$$\begin{aligned} \Gamma_{\sigma, \sigma'} &= \phi_\sigma(T) - \phi_{\sigma'}(T) \\ &= -\gamma(\sigma - \sigma') \int_0^T x(s) ds . \end{aligned} \quad (44)$$

As noted above, in the weak noise approximation, eq. (31) indicates that $a_\sigma(T)$ is determined by the noiseless QuAdS dynamics. Thus if $|\psi(0)\rangle = |\chi(0)\rangle$ is initially equal to the initial groundstate $|E_g(0)\rangle$, then $|\chi(T)\rangle = |E_g(T)\rangle$ and so $a_\sigma(T) = \langle \sigma_1 \cdots \sigma_N | E_g(T) \rangle$. Thus all noise dependence in this approximation appears in the stochastic phases $\{\phi_\sigma(T)\}$ which clearly depend on σ (see eq. (41)). The stochastic character of the noise requires us to represent our quantum system by an ensemble in which each element of the ensemble is our quantum system in the presence of a particular noise realization. As we do not know which element of the ensemble will correspond to our quantum system on a given run of QuAdS, we must average over the ensemble to determine the expected performance of QuAdS in the presence of

noise. We now show that these stochastic phases lead to a suppression of the off-diagonal matrix elements ($\sigma \neq \sigma'$) of $\rho(T)$ when the noise-average is carried out. The noise-averaged density matrix $\bar{\rho}_{\sigma, \sigma'}(T)$ is thus

$$\bar{\rho}_{\sigma, \sigma'}(T) = D_{\sigma, \sigma'} a_\sigma(T) a_{\sigma'}^*(T) , \quad (45)$$

where

$$D_{\sigma, \sigma'} = \overline{\exp[-i\Gamma_{\sigma, \sigma'}]} \quad (46)$$

is the decoherence factor. In the adiabatic limit, the thermal relaxation time (a.k.a. noise correlation time) τ satisfies $\tau \ll T$. We divide the integration interval $[0, T]$ appearing in $\Gamma_{\sigma, \sigma'}$ (eq. (44)) into $M = T/\tau$ subintervals of duration τ . This renders $\Gamma_{\sigma, \sigma'}$ into a sum of uncorrelated random variables $\Gamma_{\sigma, \sigma'}(j)$:

$$\Gamma_{\sigma, \sigma'} = \sum_{j=1}^M \Gamma_{\sigma, \sigma'}(j) , \quad (47)$$

where

$$\Gamma_{\sigma, \sigma'}(j) = -\gamma(\sigma - \sigma') \int_{(j-1)\tau}^{j\tau} x(s) ds . \quad (48)$$

Since the noise is stationary, the set of $\{\Gamma_{\sigma, \sigma'}(j)\}$ have identical probability distributions. If the $\{\Gamma_{\sigma, \sigma'}(j)\}$ are not only uncorrelated, but also statistically independent, it follows from the central limit theorem that $\Gamma_{\sigma, \sigma'}$ will have a Gaussian probability distribution with mean $\overline{\Gamma_{\sigma, \sigma'}}$ and variance $\overline{\Gamma_{\sigma, \sigma'}^2}$. From eqs. (47) and (48), and the fact that the noise $x(t)$ has zero mean $\overline{x(t)} = 0$, it follows that $\overline{\Gamma_{\sigma, \sigma'}} = 0$. From eq. (44),

$$\Gamma_{\sigma, \sigma'}^2 = \gamma^2(\sigma - \sigma')^2 \int_0^T ds \int_0^T ds' x(s)x(s') . \quad (49)$$

Averaging over the noise gives

$$\overline{\Gamma_{\sigma, \sigma'}^2} = \gamma^2(\sigma - \sigma')^2 \int_0^T ds \int_0^T ds' \overline{x(s)x(s')} . \quad (50)$$

For our noise model, the noise correlation function $\overline{x(s)x(s')}$ is (see Section III A):

$$\overline{x(s)x(s')} = \sigma_x^2 h(s - s') . \quad (51)$$

To avoid confusion with σ defined in eq. (35), we have written σ_x^2 for the variance of x-noise (denoted by σ^2 in Sections III and IV); and recall that $h(s - s')$ is our square pulse noise fluctuation profile of unit height and width 2τ . Using eq. (51) in eq. (50) and carrying out the integrations gives:

$$\overline{\Gamma_{\sigma, \sigma'}^2} = 4\tau T (\sigma - \sigma')^2 \gamma^2 \sigma_x^2 . \quad (52)$$

We now have the ingredients needed to evaluate the decoherence factor $D_{\sigma,\sigma'}$:

$$\begin{aligned} D_{\sigma,\sigma'} &= \int_{-\infty}^{\infty} \frac{d\Gamma_{\sigma,\sigma'}}{\sqrt{2\pi\Gamma_{\sigma,\sigma'}^2}} \exp\left[-\frac{\Gamma_{\sigma,\sigma'}^2}{2\Gamma_{\sigma,\sigma'}^2}\right] \exp[-i\Gamma_{\sigma,\sigma'}] \\ &= \exp\left[-\frac{\Gamma_{\sigma,\sigma'}^2}{2}\right]. \end{aligned} \quad (53)$$

Using eq. (52) gives

$$D_{\sigma,\sigma'} = \exp\left[-2\gamma^2\tau T\sigma_x^2(\sigma - \sigma')^2\right]. \quad (54)$$

A number of remarks are in order.

(1) For quantum adiabatic dynamics, $T \gg 1$. Thus for non-zero σ_x^2 , τ , and γ , the decoherence factor $D_{\sigma,\sigma'}$ is exponentially small. Thus a quantum state that is a superposition of pointer basis states will undergo an effective wavefunction collapse and $\rho(T)$ will become effectively diagonal in the pointer basis. Thus we get the standard decoherence phenomenology [20] from our noise model. As we have seen, the noisy background field $\mathbf{N}_i(t)$ generates a stochastic phase $\phi_{\sigma}(T)$ which is different for the different pointer basis states $|E_{\sigma}(t)\rangle$, and which causes suppression of the off-diagonal matrix elements of $\rho(T)$ when we average over the noise. As noted above, since one doesn't know what noise realization will appear on any particular run of QuAdS, one must noise-average to determine the impact of noise on QuAdS performance. It is worth noting that, although the original decoherence analysis [20] considers an environment which is a quantum system, it has been conventional wisdom that noise-induced dephasing can generate the usual decoherence phenomenology [21], although we are not aware of any explicit demonstration of this expectation prior to the one presented above.

(2) For QuAdS, the above analysis is relevant whenever $[H_{int}(t), H(t)] \neq 0$, since then the pointer basis states differ from the instantaneous eigenstates of $H(t)$. Since the instantaneous eigenstates must then be a superposition of the pointer basis states, they are vulnerable to the effective wavefunction collapse produced by the noise-induced decoherence discussed above. Since such an effective collapse signals the effective loss of quantum coherence, one would expect that this decoherence would jeopardize any advantage QuAdS might acquire due to the quantum nature of its dynamics. It was this naive expectation that motivated us to do a careful study of the effects of noise of QuAdS performance. To test this idea, we decided to study noise which coupled to the qubits via the Zeeman interaction (see eqn. (7)), and whose polarization was constant: $\hat{\mathbf{N}}_i(t) = \hat{\mathbf{x}}; \hat{\mathbf{y}}; \hat{\mathbf{z}}$. The pointer basis states are then, respectively, the eigenstates of direct products of the qubit Pauli operators: $\prod_{i=1}^N \otimes \sigma_x^i; \prod_{i=1}^N \otimes \sigma_y^i; \text{ and}$

$\prod_{i=1}^N \otimes \sigma_z^i$. We also recognized that such an interaction would also allow a study of what would happen if the coupling interaction generated a pointer basis that varied randomly with time. This case corresponds to our 3-noise simulation in which the noise fluctuates along all 3 directions simultaneously. Refs. [9] and [10] show that a quantum phase transition occurs during QuAdS near $t/T \sim 0.7$. Before (after) this phase transition the quantum dynamics is essentially driven by H_i (H_p). As discussed in Section II B, the eigenstates of H_i (H_p) correspond to qubit spins aligned along $\hat{\mathbf{x}}$ ($\hat{\mathbf{z}}$).

- For noise with fluctuations along $\hat{\mathbf{x}}$ and for $t/T < 0.7$, $[H(t), H_{int}(t)] \approx 0$ and the instantaneous energy eigenstates are essentially the same as the pointer basis states throughout the first 70% of the quantum evolution. Noise-induced dephasing is thus only effective during the final 30% of the evolution where $[H(t), H_{int}(t)] \neq 0$ and the pointer basis differs from the instantaneous energy eigenstates. Only during the final 30% of the quantum evolution will noise act to dephase entanglement.
- For noise fluctuations along $\hat{\mathbf{y}}$, $[H(t), H_{int}(t)] \neq 0$ for all t , and the instantaneous energy eigenstates *never* correspond to the pointer basis. Thus noise-induced dephasing occurs throughout the *entire* dynamical evolution.
- For z-type noise, $[H(t), H_{int}(t)] \approx 0$ during the final 30% of the dynamical evolution, while noise-induced dephasing occurs over the initial 70% of the evolution. Thus dephasing of entanglement occurs over nearly 3/4's of the quantum evolution.

These remarks suggest that z-type noise should have a larger impact on QuAdS than x-type noise, and that y-type noise should have the most severe impact of the three. As 3-type noise has fluctuations along all 3 directions, it is unlikely that noise fluctuations of this type will remain aligned with any one of the coordinate axes throughout the entire adiabatic evolution. Thus 3-type noise will sample the most damaging y-type fluctuations less often than y-type noise, and the more benign x-type fluctuations less often than x-type noise. As a result, one would expect 3-type noise to have a less severe impact on QuAdS than y-type noise, and more of an impact than x-type noise. This is what we see in our simulations (see Tables I–VI). We see that knowledge of the occurrence of a quantum phase transition during QuAdS near $t/T \sim 0.7$, together with knowledge of how phase decoherence degrades pointer basis superpositions, allows us to understand most of the trends in our numerical results. Applying these arguments to a comparison of 3-type noise with z-type noise does not lead to any simple conclusion as far as we can tell. Our simulation results suggest that this case is in fact less straightforward as 3-type noise is less damaging to QuAdS performance than z-type noise at the lowest power levels simulated, but becomes more

detrimental to QuAdS at the larger power levels.

(3) Using eq. (54), we can estimate the degree of decoherence in our simulations. From this formula we see that the least amount of decoherence will occur for $\sigma - \sigma' = 1$ (i. e. $D_{\sigma, \sigma'}$ is largest):

$$D_{max}^x = \exp \left[-2\gamma^2 \tau T \sigma_x^2 \right] . \quad (55)$$

For our simulations, $\sigma_x = 0.2$, $\tau = 1$, and $\gamma = 1$. For x-noise with $\bar{P} = 0.005$ and $N = 13$, $\langle T(13) \rangle \sim 22$ and $[H_{int}(t), H(t)] \neq 0$ for $0.7T \leq t \leq T$, or 30% of the time for QuAdS to be carried out. Thus only $0.3T$ should be used in eq. (55) since only for this duration did the instantaneous eigenstates of $H(t)$ differ from the pointer basis. Inserting these values into eq. (55) gives $D_{max}^x \sim 0.590$. Thus for our simulation of x-noise, QuAdS still possesses a substantial amount of quantum coherence. Repeating the above analysis for y-noise we again find eq. (54) with $\sigma_x^2 \rightarrow \sigma_y^2$. Setting $(\sigma - \sigma' = 1)$, we find:

$$D_{max}^y = \exp \left[-2\gamma^2 \tau T \sigma_y^2 \right] . \quad (56)$$

For $\bar{P} = 0.005$, $\langle T(12) \rangle \sim 35$, and $[H_{int}(t), H(t)] \neq 0$ throughout all of the QuAdS. Thus, inserting $T \sim 35$ into eq. (56), along with $\sigma_y = 0.2$, and the above values for τ and γ gives $D_{max}^y \sim 0.06$. Thus y-noise at $\bar{P} = 0.005$ produces non-trivial decoherence effects.

(4) Finally, we show that for weak noise D_{max} provides an upper bound for the noise-averaged success probability of QuAdS.

As explained in Section II B, for a USA instance of EC3, the groundstate $|E_g(T)\rangle$ of the final noiseless QuAdS Hamiltonian $H(T)$ (eq. (1)) encodes the unique solution to this instance. The probability P_{suc} for QuAdS to succeed on this instance is:

$$P_{suc} = \text{Tr } P_g \rho(T) , \quad (57)$$

where $P_g = |E_g(T)\rangle\langle E_g(T)|$ is the projection operator onto the final groundstate $|E_g(T)\rangle$ and $\rho(T) = |\psi(T)\rangle\langle\psi(T)|$ is the final density matrix. We can assess the impact of noise on the performance of QuAdS by evaluating the noise-averaged success probability $\overline{P_{suc}}$:

$$\overline{P_{suc}} = \overline{\text{Tr } P_g \rho(T)} . \quad (58)$$

Since P_g projects onto the final groundstate of the noiseless QuAdS Hamiltonian, it does not depend on noise and so:

$$\begin{aligned} \overline{P_{suc}} &= \text{Tr } P_g \overline{\rho(T)} \\ &= \sum_{\sigma, \sigma'} (a_{\sigma}(T) a_{\sigma'}^*(T)) \{ D_{\sigma', \sigma} a_{\sigma'}(T) a_{\sigma}^*(T) \} , \end{aligned} \quad (59)$$

where we: (i) have carried out the trace using the pointer basis states (eqs. (32) and (33)); and (ii) used eq. (45) and

the definition of $a_{\sigma}(T)$ given below eq. (44). Noting that the set of $\{a_{\sigma}(T) a_{\sigma'}^*(T)\}$ are the matrix elements of the density matrix $\rho_g(T) = |E_g(T)\rangle\langle E_g(T)|$ in the pointer basis representation, we have

$$\begin{aligned} \overline{P_{suc}} &= \sum_{\sigma, \sigma'} D_{\sigma', \sigma} (\rho_g(T))_{\sigma, \sigma'} (\rho_g(T))_{\sigma', \sigma} \\ &\leq D_{max} \text{Tr} (\rho_g(T))^2 \\ &\leq D_{max} . \end{aligned} \quad (60)$$

Here we have used that $\rho_g(T)$ describes a pure state so that $(\rho_g(T))^2 = \rho_g(T)$. From eqs. (55) and (56) we see that the noise-averaged success probability for QuAdS is exponentially sensitive to the noise parameters appearing in D_{max} . It is clearly of interest to extend the above analysis beyond the limit of weak noise. We leave this extension to future work.

C. Future Work

A number of directions for future work suggest themselves. As mentioned above, we would like to extend our simulations to larger noise power levels to examine: (i) how rapidly the scaling exponent b increases with noise power; (ii) the degree to which the quality of the power-law and exponential fits continues to decrease with noise power; and (iii) how the quality of the exponential-fit compares with that of the power-law fit as noise power is increased. The aim of this latter point being to see if we can observe whether one of the two types of scaling laws begins to provide a significantly better fit than the other at some higher noise power level. We would also like to examine quantitatively how QuAdS performance is affected by noise which varies from one qubit-site to another. One would expect that, for this type of noise, noise-induced decoherence would be more effective at hampering QuAdS performance than the uniform noise we have considered in this paper. It would also be interesting to extend the weak noise analysis of the upper bound on the noise-averaged success probability for QuAdS to stronger noise. Finally, Farhi et. al. [22] have argued that varying the path from H_i to H_p might improve QuAdS performance. Noise can be thought to implement a random path variation, and so it might be interesting to examine whether a noise parameter regime exists where the performance enhancement of Ref. [22] might occur. As pointed out in the Introduction, we did find noise realizations which did reduce the runtime of QuAdS on a given USA instance, but it appears that the predominant effect of noise at the power levels that we considered is to slow down QuAdS. It might be worthwhile to examine whether noise-improved QuAdS might occur at small noise power levels.

VI. SUMMARY

In this paper we have presented the results of a large-scale simulation of QuAdS in the presence of noise. We determined the noise-averaged median runtime $\langle T(N) \rangle$ for QuAdS to succeed in solving USA instances of the NP-Complete problem N-Bit Exact Cover 3. Clear evidence was found of the algorithm's sensitivity to noise. We simulated noise with 4 different types of polarization, and our results are the outcome of approximately 300,000 integrations of the Schrodinger equation. The scaling relation for $\langle T(N) \rangle$ versus the number of bits N was fit with both a power-law scaling $\langle T(N) \rangle = aN^b$ and an exponential scaling $\langle T(N) \rangle = a[\exp(bN) - 1]$. Both scaling relations provided excellent fits to the simulation results, although the quality of the fits were found to decrease slightly with increasing noise power. The quality of the exponential fit decreased at a slightly slower rate than did that of the power-law fit. The variation of the scaling parameters a and b with mean noise power and noise polarization was determined. Our simulation

results are summarized in Tables I–VI. These tables order the noise types according to which type most slowed down QuAdS. We also showed how noise-induced dephasing can cause decoherence in the dynamics of QuAdS, estimate the amount of decoherence present in our simulations of noisy QuAdS, and derive an upper bound for the noise-averaged QuAdS success probability in the weak noise limit that is appropriate for our simulations.

Acknowledgments

I would like to thank T. Howell III for continued support, the National Science Foundation for support provided through Grant No. NSF-PHY-0112335, and the Army Research Office for support provided through Grant No. DAAD-19-02-1-0051. I would also like to thank the National Center for Supercomputing Applications at the University of Illinois at Urbana-Champaign for access to the TeraGrid cluster through Grant No. PHY040024T.

-
- [1] C. H. Papadimitriou, *Computational Complexity* (Addison Wesley Longman, New York, 1994).
 - [2] P. Shor, in *Proceedings of the 35th Annual Symposium on the Foundations of Computer Science*, edited by S. Goldwasser (Los Alamitos, CA, IEEE Press, 1994), p. 124.
 - [3] C. H. Bennett et. al., *SIAM J. Comput.* **26**, 1510 (1997).
 - [4] M. A. Nielsen and I. L. Chuang, *Quantum Computation and Quantum Information* (Cambridge University Press, New York, 2000).
 - [5] E. Farhi et. al., *Science* **292**, 472 (2001).
 - [6] E. Farhi et. al., <http://arXiv.org/abs/quant-ph/0001106>.
 - [7] J. Roland and N. J. Cerf, *Phys. Rev. A* **68**, 062312 (2003).
 - [8] D. R. Mitchell et. al., <http://arXiv.org/abs/quant-ph/0409088>.
 - [9] R. Orús and J. I. Latorre, *Phys. Rev. A* **69**, 052308 (2004).
 - [10] J. I. Latorre and R. Orús, *Phys. Rev. A* **69**, 062302 (2004).
 - [11] A. M. Childs, E. Farhi, and J. Preskill, *Phys. Rev. A* **65**, 012322 (2001).
 - [12] J. Roland and N. J. Cerf, <http://arXiv.org/abs/quant-ph/0409127>.
 - [13] D. S. Johnson and C. H. Papadimitriou, in *The Traveling Salesman Problem*, E. L. Lawler et. al., Eds. (Wiley, New York, 1985), p. 37.
 - [14] A. Messiah, *Quantum Mechanics* (North-Holland, Amsterdam, 1961), vol. II.
 - [15] E. Farhi, J. Goldstone, and S. Gutmann, <http://arXiv.org/abs/quant-ph/0007071>.
 - [16] J. B. Thomas, *Statistical Communication Theory* (Wiley, New York, 1969).
 - [17] F. Rief, *Fundamentals of Statistical and Thermal Physics* (McGraw-Hill, New York, 1965).
 - [18] A. W. Drake, *Fundamentals of Applied Probability Theory* (McGraw-Hill, New York, 1967).
 - [19] S. O. Rice, *Bell Sys. Tech. J.* **23**, 282 (1944).
 - [20] W. H. Zurek, *Phys. Rev. D* **24**, 1516 (1981); *Phys. Rev. D* **26**, 1862 (1982); in *From Statistical Physics to Statistical Inference and Back*, edited by P. Grassberger and J.-P. Nadal (Kluwer, Dordrecht, 1994).
 - [21] W. H. Zurek, *Rev. Mod. Phys.* **75**, 715 (2003), see Section IVC.
 - [22] E. Farhi et. al., <http://arXiv.org/abs/quant-ph/0208135>.